Research Article Vol. 58, No. 3 / 20 January 2019 / Applied Optics 609

applied optics

Design of off-axis three-mirror systems with ultrawide field of view based on an expansion process of surface freeform and field of view

Qingyu Meng,[1,2,*] Hongyuan Wang,[2] Wenjing Liang,[3] Zhiqiang Yan,[2] and Bingwen Wang[2]

[1]Changchun Institute of Optics, Fine Mechanics and Physics, Chinese Academy of Sciences, No. 3888, Dongnanhu Road, Changchun 130033, China
[2]Research Center for Space Optical Engineering, Harbin Institute of Technology, No. 2 Yikuang Street, Harbin 150001, China
[3]College of Geo-Exploration Science and Technology, Jilin University, No. 938 Ximinzhu Street, Changchun 130026, China
*Corresponding author: mengqy@ciomp.ac.cn

Received 6 August 2018; revised 10 December 2018; accepted 11 December 2018; posted 12 December 2018 (Doc. ID 341504); published 17 January 2019

Unobscured reflective optical systems with a wide field of view (FOV) have significant application values. However, the aberration increases with the increase of the system FOV, so a wide FOV system is difficult to design. In this paper, a design method that is effective in achieving off-axis three-mirror systems with ultrawide FOV is proposed. In this method, the system FOV is expanded stepwise in the design process, and the surface optical freeform polynomial terms are extended based on the judgment of image quality and some constraint conditions, and to obtain a prospective ultrawide FOV system. A freeform off-axis three-mirror imaging system with a focal length of 1000 mm, an F-number of 10, and an ultrawide FOV of 80° × 4° is designed as an example. This design result shows that the system has a high imaging quality of RMS wavefront error value of $0.040\lambda(\lambda = 0.633\ \mu m)$, and it demonstrates that the method is effective in achieving off-axis three-mirror systems with an ultrawide FOV.

https://doi.org/10.1364/AO.58.000609

1. INTRODUCTION

Off-axis unobscured optical systems have been applied in various telescopes due to their advantages of better spot diagram energy concentration and improved observation frequency of specified target areas. Some famous telescope projects, such as the Advanced Technology Large-Aperture Space Telescope (ATLAST), the Wide-Field Infrared Survey Telescope (WFIRST), and other projects all have planned off-axis unobscured optical system schemes [1–3]. Unlike the survey telescopes, due to the advantage of achieving much wider linear fields of view (FOVs), off-axis unobscured optical systems have been also widely applied in optical remote sensors. Push-broom imaging is a frequent application mode of optical remote sensing in ground sampling. The larger FOV will obtain a much wider swath, which is a significant performance index of the optical remote sensor. An off-axis unobscured optical system with a wide linear FOV has a greater application advantage in optical remote sensing.

In order to obtain a wide FOV in off-axis unobscured optical systems, researchers have done a great deal of work and attained some achievements. Meng has designed an off-axis three-mirror-anastigmatic (TMA) system with an FOV of 30° × 1° [4]; Zhu has designed an off-axis TMA system with an ultrawide FOV of 70° × 1° [5]; Zhang has designed an off-axis four-mirror system with an FOV of 76° × 1°, and in that system, a 790 mm × 390 mm concave high-gradient freeform surface mirror and a 100 mm × 100 mm convex freeform surface mirror have been manufactured [6]; David has designed an off-axis two-mirror system with an FOV of 108° [7]; a summary of the above systems' parameters is shown in Table 1. It is known in aberration theory that an FOV increase will result in an exponential growth in the aberration. To balance the wavefront and obtain good image quality, optical freeform surfaces, which are regarded as an efficient method, are applied on the mirrors without exception among these large FOV systems. Optical freeform surfaces are a catalog of nonrotational symmetric surfaces, and they have strong aberration correction ability that is realized by their multi-degrees of freedom (DOFs) rather than by the conventional optical surfaces [8]. To apply optical freeform to achieve high-performance optical systems, multiple optical freeform design methods have been proposed, such as the differential equation method [9–12], simultaneous multiple-surface (SMS) method [13,14], construction and iteration (C-I) method [15–17], and so on.

In this paper, a common design method with an expansion process of surface freeform polynomial terms and FOV (ESF) is

Table 1. Parameters Summary of Some Off-Axis Systems with Wide FOV

NO.	FOV	F-number	Focal Length	Configuration Type
1	30° × 1°	12	1200 mm	off-axis three-mirror
2	70° × 1°	5.8	75 mm	off-axis three-mirror
3	76° × 1°	6.5	550 mm	off-axis four-mirror
4	108° × 0.29°	unknown	unknown	off-axis two-mirror

proposed to achieve freeform off-axis TMA systems with ultrawide FOV. Based on this efficient design method, an off-axis TMA system with a focal length of 1000 mm, an F-number of 10, and an ultrawide FOV of 80° × 4° is achieved as an example. We believe that this system is the largest FOV TMA system with a focal length of 1 m level that has been published so far.

2. DESIGN METHOD WITH AN EXPANSION PROCESS OF SURFACE FREEFORM POLYNOMIAL TERMS AND FOV (ESF)

The core ideology of the ESF method is expanding the system FOV stepwise in the design process, and the surface optical freeform polynomial terms are extended based on the judgment of image quality and some constraint conditions in order to obtain a prospective ultrawide FOV system. A detailed flow diagram of the ESF method is shown in Fig. 1.

As with most design methods, the optical system initial configuration is established at the beginning. An off-axis TMA system can be evolved from a coaxial TMA by offset aperture or an FOV offset process, and it also can be established by the direct calculation method [18]. As mentioned above about the FOV expanding, to obtain an ultrawide FOV, a small FOV is set in the initial configuration, and the merit function is decided according to the requirements. Usually, the wavefront error (WFE) is chosen as the merit function; other criteria, such as MTF or PSF and so on, also can be chosen. The configuration constraint conditions should be set before optimization.

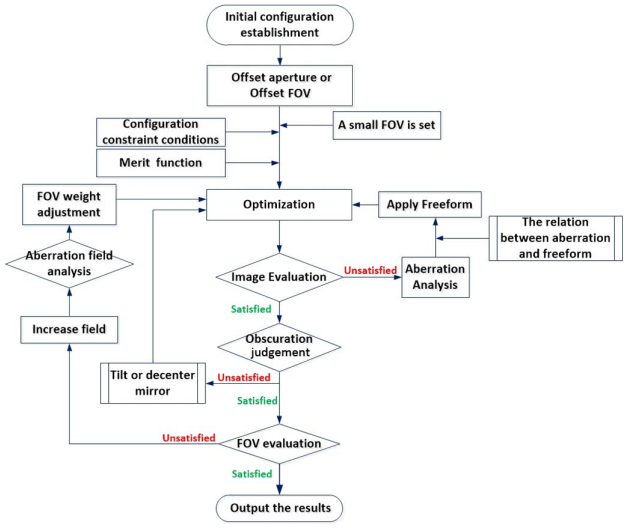

Fig. 1. Flow diagram of ESF method for designing off-axis TMA system with ultrawide FOV.

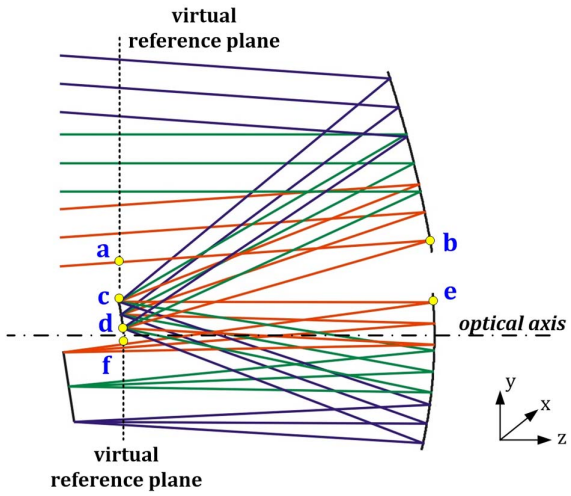

Fig. 2. One-dimensional ray-tracing constraints condition for the small FOV system.

A. Beam Footprint Definition of Configuration Constraint Condition

The configuration constraint condition mainly includes system size restrictions and mirror intervention caused by mirror or ray crossing, which is significant for an off-axis TMA system. For a small FOV system, the ray-restriction conditions are always illustrated in a one-dimensional tangential plane, shown in Fig. 2. Generally, some feature points are chosen, and their coordinate should satisfy Eq. (1):

$$\begin{cases} y_a > y_c \\ y_b > y_e \\ y_d > y_f \end{cases}, \tag{1}$$

where $y_a, y_b, y_c, y_d, y_e, y_f$, are the coordinates in the y direction of specific points of the intersection points of the ray with mirrors or virtual surfaces.

However, for a wide FOV system, the ray coordinates in the y direction for every field that has the same tangential field value on the same mirror have great differences due to distortion. As shown in Fig. 3, because of the distortion, the

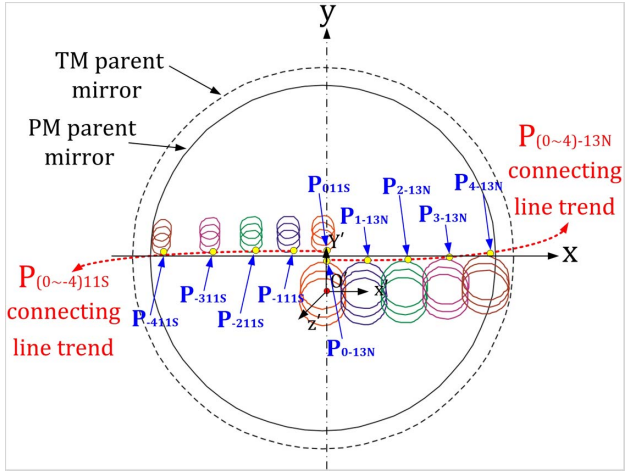

Fig. 3. 2D ray-tracing constraints condition for the ultrawide FOV system.

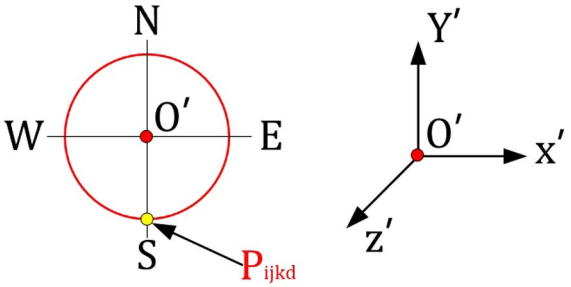

Fig. 4. Beam footprint definition of the mirror or virtual plane.

coordinates of the beam footprint of every field that has the same tangential field value on the same mirror are different in the y direction. It shows that the one-dimensional ray-tracing constraints condition are insufficient, so it is necessary to propose a ray-tracing constraint for the wide FOV system.

Here, we propose a beam footprint definition of the mirror or virtual plane.

A Cartesian coordinate system $x'y'z'$ is defined where the x' axis, y' axis, and z' axis are parallel to the optical system coordinate system x axis, y axis, and z axis, respectively. O' is the original point of the $x'y'z'$ coordinate system, and it is also the center point of the beam footprint on every mirror.

P_{ijkd} is the intersection point of the beam footprint with an $x'y'z'$ coordinate axis, as shown in Fig. 4, where i is the field number in the x direction (the sign is according to the coordinate axis direction, and the center field number is 0), j is the field number in the y direction (the sign is according to the coordinate axis direction, and the center field number is 0), k is the mirror or the virtual plane number, d is the intersection point orientation about the coordinate axis, and we use N, S, W, E to represent the orientation.

Based on the above definitions about beam footprint, if five fields of semi-FOV are defined in the x direction in the design process for a TMA system, as shown in Fig. 3, to avoid mirror intervention of the primary mirror (PM) and tertiary mirror (TM), the two-dimensional (2D) ray-tracing constraints conditions should be as in Eq. (2). Based on Eq. (2), some margins also should be included, because any real optomechanical design requires air gaps and free space to place holders and align the optics:

$$P_{(0\sim-4)11S} > P_{(0\sim4)-13N}. \tag{2}$$

B. Optimization Process

The system optimization is started after the above preparatory work. In the ESF method, the optical surface is complicated stepwise, based on the judgment of image quality and some constraint conditions, so the surface type should be kept simple in the initial system. After every round of optimization, the optical system will be evaluated from multiple criteria, and the evaluation has a direct impact on the optimization strategy in the next step:

(a) Following the optimization, the image quality is evaluated first; if it is not satisfied with the criteria, the aberration field will be analyzed, and based on the quantitative and qualitative relations between aberration and freeform polynomial terms, optical freeform can be applied on the mirror. If the aberration can be corrected well by some simple surface such as an asphere, then the complicated freeform should not be selected first.

When the freeform surface is at the pupil position, the beam footprint on the surface is the same for all the fields, so all fields receive the same wavefront contributions from the freeform surface, and the system obtains the one-to-one aberration compensation corresponding to the freeform polynomial terms. When the freeform surface is not at the pupil position, different fields receive the different wavefront contributions from the freeform surface. The wavefront contribution relation of the freeform and freeform polynomial terms application principle are combined with qualitative and quantitative analysis [19,20].

The application of the freeform is under the guidance of the analysis of system aberration field distribution and the qualitative and quantitative aberration correction ability of every freeform polynomial term. In the design process of freeform terms, the number of freeform terms is expanded from few to more, and the power of freeform terms is expanded from low to high.

(b) If the image quality is satisfied with the criteria, the obscuration will be judged. When there is obscuration in the system, tilt and decenter will be applied on the mirror to avoid ray obscuration.

(c) When there is no obscuration, the FOV will be judged. If the FOV is not satisfied with the requirement, the FOV will be expanded and optimized. In the process, the aberration field will be analyzed, and the FOV weight can be adjusted before optimization.

In the optimization process, the error function type can be chosen as transverse ray aberration or WFE variance, and so on. These optimization algorithms are widely used in optical system design software, such as CODE V.

With the ESF design method and the 2D ray-tracing constraints condition, a design example will be given. An ultrawide FOV off-axis TMA system will illustrate the ESF method's effectiveness.

3. DESIGN OF OFF-AXIS THREE-MIRROR SYSTEMS WITH ULTRAWIDE FOV WITH ESF DESIGN METHOD

Relayed COOK TMA and nonrelayed COOK TMA are two types of widely used off-axis TMA optical systems [21]. Because the secondary mirror (SM) is set as the aperture stop, the PM and TM are symmetrical relative to the SM, so the nonrelayed COOK TMA system is capable of achieving a large FOV, shown in Fig. 5. It is chosen as the optical system configuration.

Designing a long focal length reflective system with an ultrawide FOV is a challenge. The design example has a focal length of 1000 mm, an F-number of 10, and a ultra-FOV of 80° × 4°. This optical system can be used in a push-broom optical remote

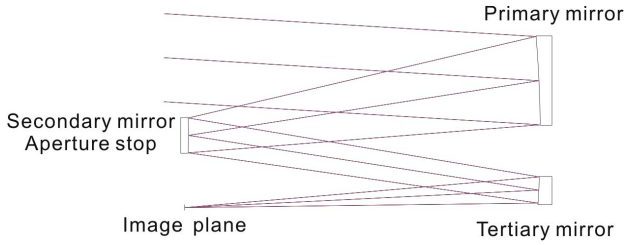

Fig. 5. Nonrelayed TMA optical system.

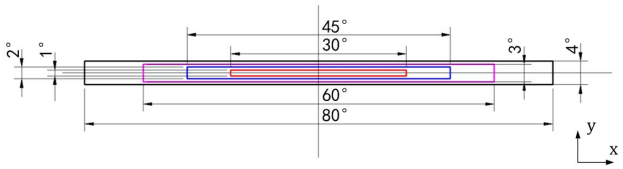

Fig. 6. FOV expansion in design process.

sensor, and with the advantage of its ultra-FOV, the remote sensor can achieve a wider swath.

Similar to many visible optical remote sensors, such as WorldView2, GeoEye1, and so on, the optical system panchromatic spectrum band can be set at 450–800 nm [22–24]. Compared with WorldView2's 770 km orbit altitude, when the optical system is coupled with the 6.5 μm pixel size time delay integration (TDI) CCD, it can achieve a resolution with 50 m, and its image swath can reach about 1300 km. Based on the detector sampling principle, the Nyquist frequency is about 77 lp/mm, and the optical system diffraction limitation is about 0.4. Based on our engineering experience, the remote sensor MTF can achieve about 0.1 at the Nyquist frequency after the MTF deterioration, which was caused by system manufacture, alignment, detector MTF, and so on.

As mentioned, in the ESF method, the system FOV is expanded step-by-step in the design process; the FOV expansion program is shown in Fig. 6. The FOV expansion process is formed in two directions: the sagittal FOV expands from ±15°, ±22.5°, ±30° to ±80°, and the tangential FOV expands from ±0.5°, ±1.0°, ±1.5° to ±2.0°. The expansion program can be adjusted by the designer. Based on experience, the central FOV in the tangential direction of the nonrelayed TMA optical system is not 0°; in the design example, the center FOV in the tangential direction is set at −7°.

According to the design planning and ESF design method, the configuration constraint conditions and merit function are set. In the configuration constraint conditions, the overall system length and 2D ray-tracing constraints condition have been set. The system RMS WFE is set as the merit function, and the RMS WFE value criterion is less than $0.040\lambda(\lambda = 0.633\ \mu m)$.

The WFE image quality criterion in the design method is not irreplaceable, and according to the corresponding requirements, the criterion also can be MTF or PSF. Because the interference testing method is an authoritative method for optical system testing, the WFE image quality criterion is applicable. Based on the Maréchal criterion, the optical system should better achieve an image quality of RMS $\lambda/14$ for most optical remote sensors. Based on our engineering experience, in the nonrelayed COOK TMA system, the PM and TM random RMS surface errors (RSEs) can achieve up to $\lambda/55$, and the SM RSE can achieve up to $\lambda/80$, which benefits from its circular rotational symmetry structure and relatively small size. Using the root of sum of squares (RSS) method to allocate system tolerance, the optical system WFE is about

$$\sqrt{\underbrace{(0.04\lambda)^2}_{\text{design residual error}} + \Big(2\times \underbrace{\lambda/55}_{\text{PM shape error}}\Big)^2 + \Big(2\times \underbrace{\lambda/80}_{\text{SM shape error}}\Big)^2 \Big(2\times \underbrace{\lambda/55}_{\text{TM shape error}}\Big)^2} = 0.069\lambda. \tag{3}$$

The other allocation margin can be left for alignment.

What should be mentioned is that the image quality criterion limited value is just a manmade set value in this paper, and the purpose of the threshold setting is to reflect and verify the design method's effectiveness.

In addition, the mirror distance is set as a controls parameter, and its value is smaller than the system focal length.

Freeform surfaces are a category of nonrotational symmetric surfaces, and freeform surfaces can be defined as global descriptions, local descriptions, and nonuniform rational *B*-splines. In these freeform surfaces, *xy* polynomials were the first type of polynomials used for low-order freeform surfaces historically and still remain a common surface description of freeform surfaces, although their nonorthogonal character leads to design complexity increases that require more than a few lower-order terms [25–27].

In our previous work, we have applied the *xy* polynomials in some TMA systems, and we have obtained some quantitative and qualitative relations between aberration and *xy* polynomial terms that are a benefit for aberration correction [4]. In addition, the *xy* polynomial surface is more convenient to establish than the symmetric surface type. In the design process, the *xy* polynomial surface is selected as the mirror freeform type, and only even order terms of *x* are retained; then the system imaging quality is symmetrical about the tangential plane, which is convenient for system alignment.

The xy polynomial surface is defined by a series of polynomials added to a base conic. The polynomial is expanded into monomials of $x^m y^n$. The equation used is

$$z = \frac{cr^2}{1 + \sqrt{1 - (1 + k)c^2 r^2}} + \sum_{j=2}^{66} C_j x^m y^n, \tag{4}$$

where z is the sag of the surface parallel to the optical-axis, c is the vertex curvature, k is the conic constant, and $x^m y^n$ is the coefficient of the monomial.

In design process, a nonrelayed COOK TMA with a FOV of 30° × 1° is designed first. The system is relatively easy to achieve; it has evolved from our previous design result [4], and it is marked as system A. The system A has an RMS WFE value of 0.027λ. In system A, the PM surface type is aspherical, and sixth and eighth coefficients are employed; the TM surface type is an *xy* polynomial surface, and the highest power is up to y^6, which is the No. 27 monomial. System A is the foundation design to achieve the ultra-FOV TMA system using the principles of the ESF design method.

Based on system A, the FOV is expanded to 45° × 2°, and the new system is marked as system B. A large amount of residual aberration exists on the edge of the FOV, so the system RMS WFE value increases from 0.027λ to 0.540λ, due to the FOV expansion. After the first round of optimization, the

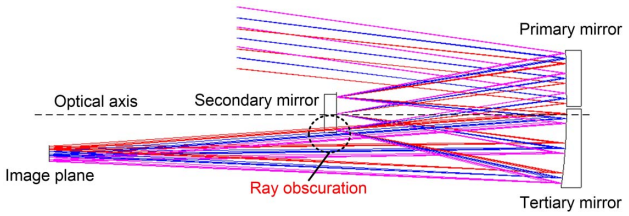

Fig. 7. Aperture obscuration in design process.

WFE is reduced to 0.057λ, and after the second round of the optimization, the WFE is reduced to 0.040λ. However, in the design result, although the RMS WFE has been further reduced with the optimization, the SM has the aperture obscuration to the ray in the back focal length region, which causes system vignetting, as shown in Fig. 7. To solve the ray obscuration, the SM and TM has been tilted 0.5°. Based on the aberration theory, the mirror tilt will generate a large amount of aberration; then the system RMS WFE value increases from 0.040λ to 8.805λ, due to the mirror position misalignment. After another round of optimization, the WFE is reduced just to 0.064λ, which still cannot meet the criterion. By analysis, there is a lot of astigmatism in the residual aberration, and by previous study [4], the terms "x^2," "xy," "y^2," "x^6," "x^5y," "x^3y^3," "xy^5," and "y^6" in the xy freeform polynomial surface are very useful to correct astigmatism. We will try to use these surface terms to correct system aberration.

Using the principles of the ESF design method, to obtain much stronger aberration ability, the PM surface type is switched from aspherical to an xy polynomial. After optimization, the PM highest power is up to x^6, which is the No. 21 monomial, and the TM highest power is up to y^6, which is the No. 27 monomial. After optimization with the ESF method, system B's RMS WFE value reaches 0.037λ, and the system astigmatism has been well corrected. The optimization process from system A to system B with the ESF design method is shown Fig. 8, which illustrates a typical optical system design process with the ESF design method. The design process and the result show that the method is effective and practical, and it is convenient for the designer to achieve a wide FOV TMA system. In addition, for ease in understanding, the

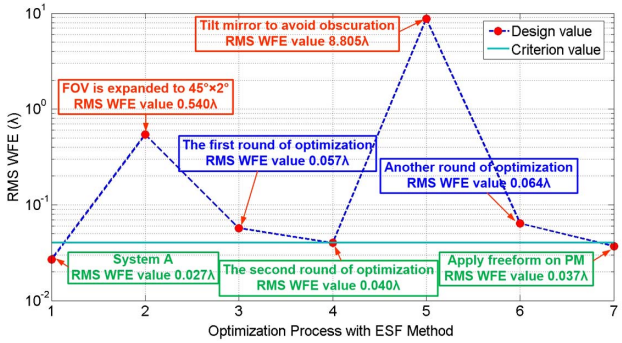

Fig. 8. Optimization process from system A to system B with the ESF design method.

Table 2. Optimization Process from System A to System B with the ESF Design Method by Table Description

Optimization Process Step	Optimization Description	RMS WFE (λ)
1	optimization starting point by system A	0.027
2	FOV is expanded to 45° × 2°	0.540
3	first round of optimization	0.057
4	second round of optimization, and obscuration occurs in the system	0.040
5	SM and TM has been tilted 0.5° to avoid obscuration	8.805
6	another round of optimization	0.064
7	apply freeform on PM	0.037

optimization process illustrated in Fig. 8 is also described in Table 2.

Similar with the system B design process, the system FOV is further expanded to 60° × 3°, as planned, and the new system is marked as system C. The system RMS WFE value increases from 0.037λ to 0.106λ, due to the FOV expansion. To correct system aberration, the PM freeform highest power has been increased. After optimization, the PM and TM highest powers are all up to y^6, which is the No. 27 monomial, and system RMS WFE value is 0.045λ, which still does not satisfy the criterion, which is less than 0.040λ. The ESF method core is an optimization expansion process of surface freeform and FOV. So, to further correct system residual aberration, the TM highest power is expanded to y^7, which is the No. 35 monomial. After optimization with the ESF method, system C's RMS WFE value reaches 0.027λ.

To achieve the ultimate purpose of FOV size, the FOV is expanded to 80° × 4° from 60° × 3°, and the new system is marked as system D. System D has an RMS WFE value of 0.336λ. Using the ESF design method, the PM and TM highest powers are all up to y^7, which is the No. 35 monomial, and the system's RMS WFE value is 0.040λ after optimization. The configuration parameters and mirror parameters are shown in Tables 3–5.

System D has a long focal length of 1000 mm, and an ultrawide FOV of 80° × 4°; the sagittal direction (x direction) FOV is 80°, where the range is from −40° to 40°, and the tangential direction (y direction) FOV is 4°, where the range is from −5° to −9°. The optical system has a high imaging quality of an RMS WFE value of 0.040λ, shown in Fig. 9. The realization of the system demonstrates the effectiveness of the ESF method.

The distortion value is large in the ultrawide FOV system, and the grid distortion data show that the grid distortion maximum value is −28.77%; the grid distortion scheme is shown in Fig. 10.

The distortion is a fixed value; in the design stage or future manufacturing stage, the system distortion can be measured accurately. Based on the measured value, the distortion can be corrected after system alignment [28].

In the design process, four stage design systems (system A, system B, system C, and system D) are generated, which are shown in Fig. 11. The 2D top-down optical system scheme is shown in Fig. 12.

Table 3. Configuration Parameters of System D

	Surface Type	Radius (mm)	Thickness (mm)	Conic	Tilt on the x axis (°)	Off-axis magnitude (mm)	Mirror size (mm)
PM	xy polynomial	−3223.08	−800.00	−7.883	0.00	100	1480 × 170
SM	conic	−1574.07	800.00	0.601	−1.00	0	Φ90
TM	xy polynomial	−1513.25	−1014.00	−0.064	1.00	−117	1400 × 260
Image plane	—	—	—	—	−4.39	−8849	1120 × 110

Table 4. PM Surface Parameters of System D

Term	Coefficient	Term	Coefficient	Term	Coefficient
x^2	1.3076e-04	y^4	−8.2293e-12	x^2y^4	2.5634e-17
y^2	1.3767e-04	x^4y	3.4034e-15	y^6	5.3207e-17
x^2y	1.1076e-08	x^2y^3	4.4538e-15	x^6y	2.7800e-21
y^3	1.3121e-08	y^5	−1.0561e-15	x^4y^3	6.1792e-21
x^4	−9.1493e-12	x^6	5.8778e-18	x^2y^5	−6.3934e-22
x^2y^2	−1.3868e-11	x^4y^2	1.9397e-17	y^7	−8.9944e-20

Table 5. TM Surface Parameters of System D

Term	Coefficient	Term	Coefficient	Term	Coefficient
x^2	3.1230e-05	y^4	6.1628e-12	x^2y^4	6.2161e-19
y^2	2.9334e-05	x^4y	−3.4364e-16	y^6	7.5499e-17
x^2y	−2.2309e-09	x^2y^3	−1.3013e-15	x^6y	−6.0073e-22
y^3	−1.8310e-09	y^5	2.3788e-14	x^4y^3	−1.7786e-21
x^4	2.8596e-12	x^6	−1.2616e-19	x^2y^5	−9.1570e-23
x^2y^2	4.7232e-12	x^4y^2	3.0917e-19	y^7	9.0962e-20

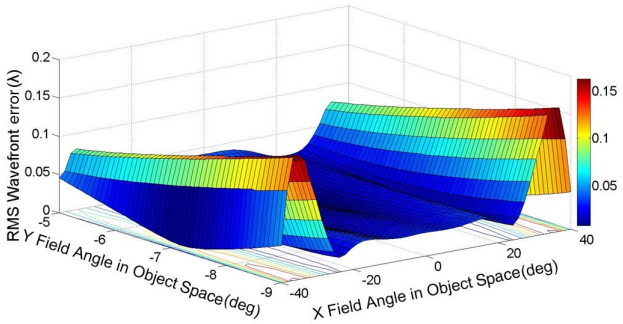

Fig. 9. WFE ($\lambda = 0.633$ μm).

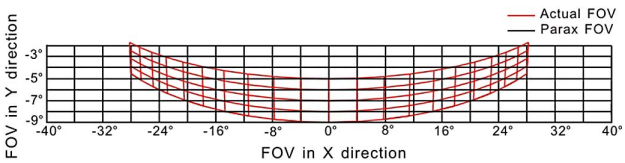

Fig. 10. Distortion grid (x FOV semi-field, 40°; y FOV semi-field, 9°).

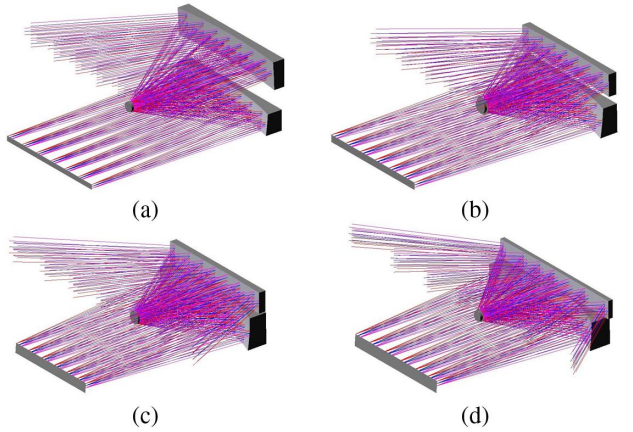

Fig. 11. Optical system scheme of (A) system A, (B) system B, (C) system C, and (D) system D.

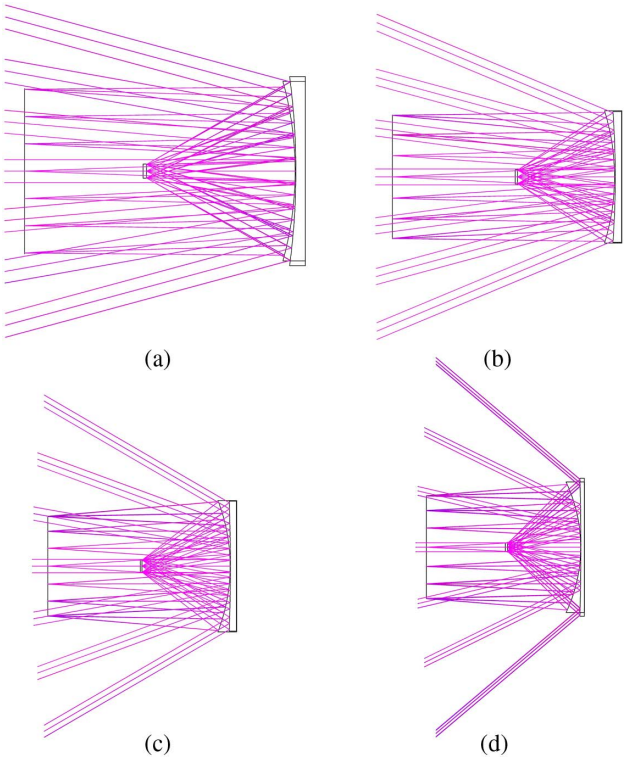

Fig. 12. 2D top-down optical system scheme of (A) system A, (B) system B, (C) system C, (D) system D.

4. CONCLUSION

In this work, a design method with an expansion process of surface freeform and FOV is proposed. The method is effective and practical in achieving freeform off-axis TMA systems with an ultrawide FOV. Based on the ESF design method, an off-axis TMA system with the focal length of 1000 mm, an F-number of 10, and an ultrawide FOV of 80° × 4° is achieved. This design result shows that the system has a high imaging quality, with an RMS WFE value of 0.040λ. The realization of the system demonstrates the effectiveness of the ESF method. We believe this system is the largest FOV TMA system with a focal length of 1 m that has been published so far.

There is still some further research we will do on the design method in the next stage. The first is to develop the design method to reduce the distortion of the ultrawide FOV TMA systems, and the other task is to set up assessment of system testability and manufacturability in this design method.

Funding. National Natural Science Foundation of China (NSFC) (61705220); ShuGuang Talents Scheme Award of CIOMP; Strategic Priority Research Program of Chinese Academy of Sciences (CAS)

REFERENCES

1. H. P. Stahl, M. Postman, W. R. Arnold, R. C. Hopkins, L. Hornsby, G. E. Mosier, and B. A. Pasquale, "ATLAST-8 Mission concept study for 8-meter monolithic UV/optical space telescope," Proc. SPIE **7731**, 77312N (2010).
2. D. Spergel, N. Gehrels, J. Breckinridge, M. Donahue, A. Dressler, B. S. Gaudi, T. Greene, O. Guyon, C. Hirata, J. Kalirai, N. J. Kasdin, W. Moos, S. Perlmutter, M. Postman, B. Rauscher, J. Rhodes, Y. Wang, D. Weinberg, J. Centrella, W. Traub, C. Baltay, J. Colbert, D. Bennett, A. Kiessling, B. Macintosh, J. Merten, M. Mortonson, M. Penny, E. Rozo, D. Savransky, K. Stapelfeldt, Y. Zu, C. Baker, E. Cheng, D. Content, J. Dooley, M. Foote, R. Goullioud, K. Grady, C. Jackson, J. Kruk, M. Levine, M. Melton, C. Peddie, J. Ruffa, and S. Shaklan, "Wide-field infrared survey telescope-astrophysics focused telescope assets WFIRST-AFTA final report," arXiv:1305.5422 (2013).
3. X. Zhang, J. Zhang, L. Wang, and G. Shi, "Optical design of off-axis astronomical telescope based on freeform surfaces," in *Classical Optics*, OSA Technical Digest (Optical Society of America, 2014), paper ITh2A.2.
4. Q. Meng, H. Wang, K. Wang, Y. Wang, Z. Ji, and D. Wang, "Off-axis three-mirror freeform telescope with a large linear field of view based on an integration mirror," Appl. Opt. **55**, 8962–8970 (2016).
5. W. Hou, J. Zhu, T. Yang, and G. Jin, "Construction method through forward and reverse ray tracing for a design of ultra-wide linear field-of-view off-axis freeform imaging systems," J. Opt. **17**, 055603 (2015).
6. X. Zhang, L. Zheng, X. He, L. Wang, F. Zhang, S. Yu, G. Shi, B. Zhang, Q. Liu, and T. Wang, "Design and fabrication of imaging optical systems with freeform surfaces," Proc. SPIE **8486**, 848607 (2012).
7. D. Nijkerk, B. V. Venrooy, P. V. Doorn, R. Henselmans, F. Draaisma, and A. Hoogstrate, "The TROPOMI telescope," Proc. SPIE **10564**, 105640Z (2017).
8. T. Yang, G. Jin, and J. Zhu, "Automated design of freeform imaging systems," Light: Sci. Appl. **6**, e17081 (2017).
9. W. Tai and R. Schwarte, "Design of an aspherical lens to generate a homogenous irradiance for three-dimensional sensors with a light-emitting-diode source," Appl. Opt. **39**, 5801–5805 (2000).
10. J. Zhu, X. Wu, T. Yang, and G. Jin, "Generating optical freeform surfaces considering both coordinates and normals of discrete data points," J. Opt. Soc. Am. A **31**, 2401–2408 (2014).
11. R. A. Hicks, "Controlling a ray bundle with a free-form reflector," Opt. Lett. **33**, 1672–1674 (2008).
12. R. A. Hicks and C. Croke, "Designing coupled free-form surfaces," J. Opt. Soc. Am. A **27**, 2132–2137 (2010).
13. J. C. Miñano, P. Benítez, W. Lin, J. Infante, F. Muñoz, and A. Santamaría, "An application of the SMS method for imaging designs," Opt. Express **17**, 24036–24044 (2009).
14. F. Duerr, P. Benítez, J. C. Miñano, Y. Meuret, and H. Thienpont, "Analytic free-form lens design in 3D: coupling three ray sets using two lens surfaces," Opt. Express **20**, 10839–10846 (2012).
15. T. Yang, J. Zhu, X. Wu, and G. Jin, "Direct design of freeform surfaces and freeform imaging systems with a point-by-point three-dimensional construction-iteration method," Opt. Express **23**, 10233–10246 (2015).
16. T. Yang, J. Zhu, and G. Jin, "Design of a freeform, dual fields-of-view, dual focal lengths, off-axis three-mirror imaging system with a point-by-point construction-iteration process," Chin. Opt. Lett. **14**, 100801 (2016).
17. T. Yang, G. Jin, and J. Zhu, "Design of image-side telecentric freeform imaging systems based on a point-by-point construction-iteration process," Chin. Opt. Lett. **15**, 062202 (2017).
18. Q. Meng, H. Wang, W. Wang, and Z. Yan, "Desensitization design method of unobscured three-mirror anastigmatic optical systems with an adjustment-optimization-evaluation process," Appl. Opt. **57**, 1472–1481 (2018).
19. D. A. Atchison, D. H. Scott, and M. J. Cox, "Mathematical treatment of ocular aberrations: a user's guide," in *Vision Science and Its Applications*, V. Lakshminarayanan, ed., Vol. **35** of OSA Trends in Optics and Phototonics (Optical Society of America, 2000), pp. 110–130.
20. Q. Meng, H. Wang, and Z. Yan, "Residual aberration correction method of the three-mirror anastigmat (TMA) system with a real exit pupil using freeform surface," Opt. Laser Technol. **106**, 100–106 (2018).
21. L. G. Cook, "The last three-mirror anastigmat (TMA)?" in *Critical Reviews of Optical Science and Technology* (SPIE, 1992), Vol. **CR41**, pp. 310–324.
22. C. Padwick, M. Deskevich, F. Pacifici, and S. Smallwood, "WorldView-2 pan-sharpening," in *ASPRS Annual Conference* (2010), Vol. **2630**.
23. "GeoEye-1," https://dg-cms-uploads-production.s3.amazonaws.com/uploads/document/file/97/DG_GeoEye1.pdf.
24. "WorldView-2," https://dg-cms-uploads-production.s3.amazonaws.com/uploads/document/file/98/WorldView2-DS-WV2-rev2.pdf.
25. J. Reimers, A. Bauer, K. P. Thompson, and J. P. Rolland, "Freeform spectrometer enabling increased compactness," Light: Sci. Appl. **6**, e17026 (2017).
26. I. Kaya, K. P. Thompson, and J. P. Rolland, "Comparative assessment of freeform polynomials as optical surface descriptions," Opt. Express **20**, 22683–22691 (2012).
27. J. Ye, L. Chen, X. Li, Q. Yuan, and Z. Gao, "Review of optical freeform surface representation technique and its application," Opt. Eng. **56**, 110901 (2017).
28. K. Seidl, J. Knobbe, and H. Grüger, "Design of an all-reflective unobscured optical-power zoom objective," Appl. Opt. **48**, 4097–4107 (2009).